Supplementary information to

Transformative Chelation Pathways Unveiling NiMOF-LDH Hybrids on MgO for High-Efficiency Photocatalysis

Mohammad Aadil[1], Ananda Repycha Safira[1], Mohammad Alkaseem[2], Taekjib Choi[3], Mosab Kaseem[1,*]

[1]Corrosion and Electrochemistry Laboratory, Department of Nanotechnology and Advanced Materials Engineering, Sejong University, Seoul 05006, Republic of Korea

[2]Owlstone Medical, Cambridge CB4 0GJ, United Kingdom

[3]Hybrid Materials Research Center and Department of Nanotechnology and Advanced Materials Engineering, Sejong University, Seoul 05006, Republic of Korea

[*]Corresponding author Email: mosabkaseem@sejong.ac.kr (M. Kaseem)

Table S1. Pseudo-second order reaction kinetic calculations for Rhd B and TC photodegradation.

Sample	Rhodamine B		Tetracycline	
	Reaction rate (min^{-1})	R^2	Reaction rate (min^{-1})	R^2
MgO	0.01997 ± 0.00438	0.897	0.00379 ± 9.10289E-4	0.862
NiMOF+EDTA	0.0956 ± 0.01248	0.959	0.00451 ± 8.58755E-4	0.906
NiMOF-EDTA	0.14018 ± 0.03298	0.885	0.00574 ± 9.74999E-4	0.923
EDTA-NiMOF	0.86901 ± 0.2366	0.854	0.01072 ± 0.00142	0.951

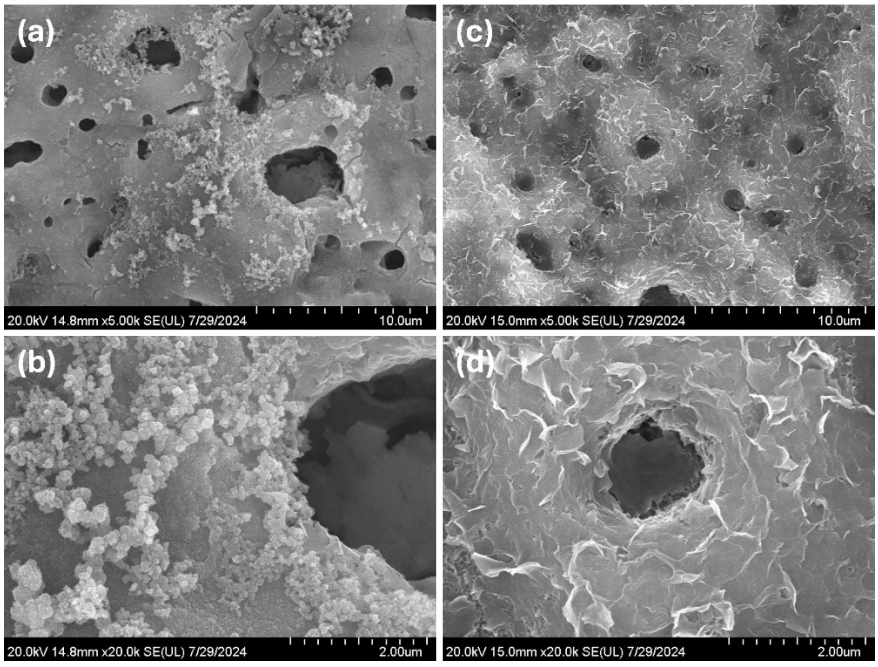

Fig. S1. Surface morphology of (a, b) EDTA on MgO surface, and (c, d) NiMOF on MgO surface.

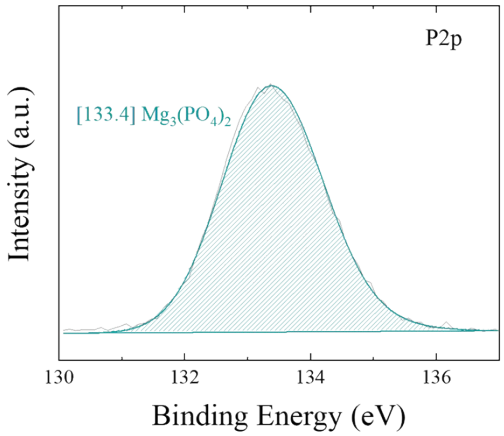

Fig. S2. Deconvoluted XPS spectra of phosphorus (2p) peak.

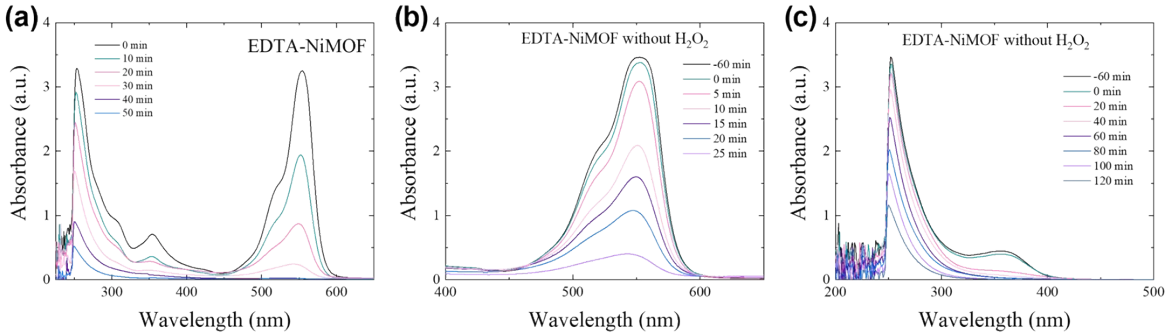

Fig. S3. Assessment of photodegradation of a mixture of 20 ml Rhd B and 20 ml TC, using EDTA-NiMOF sample.

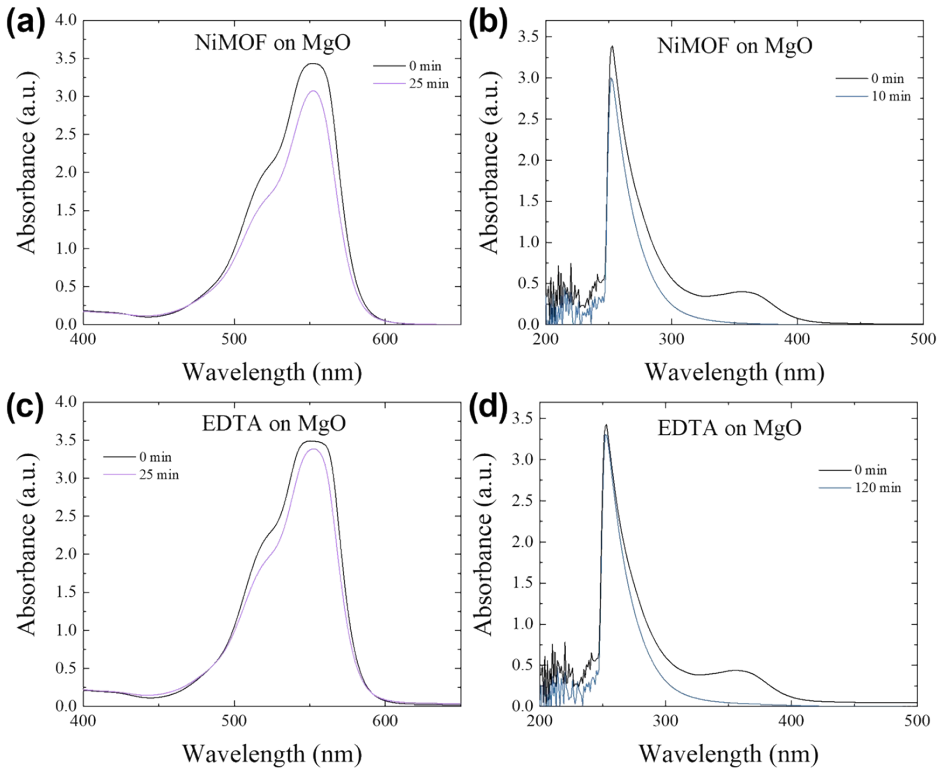

Fig. S4. Photocatalytic degradation of Rhd B and TC using (a, b) NiMOF on MgO, and (c, d) EDTA on MgO

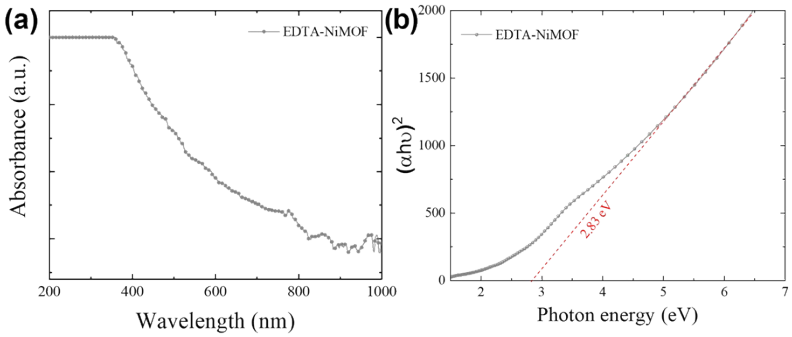

Fig. S5. (a) UV-DRS spectra, and (b) Tauc plot of EDTA-NiMOF sample.

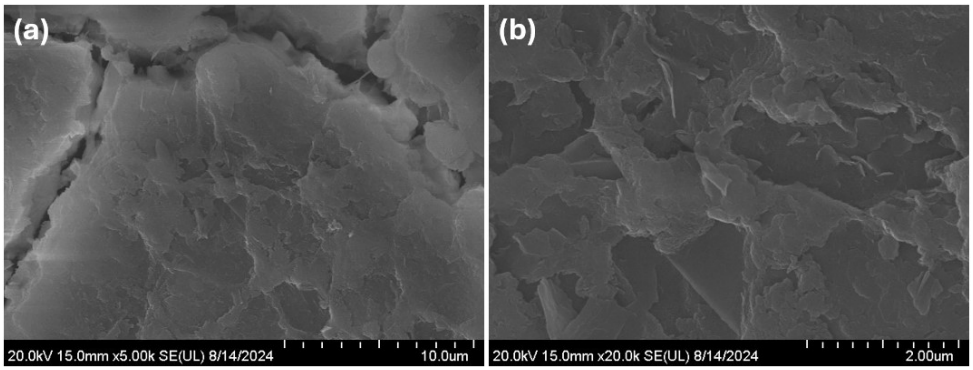

Fig. S6. Surface morphology of the best conditions i.e., EDTA formation in 1st step, and NiMOF formation in 2nd step, on AZ31 magnesium alloy substrate.

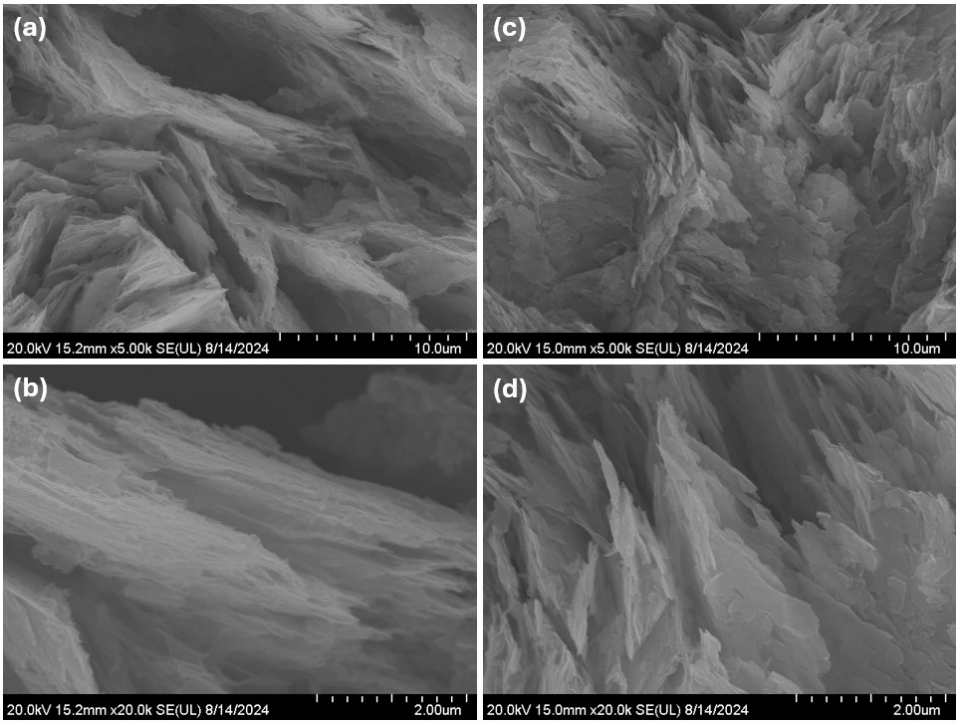

Fig. S7. Surface morphology after five cycles of photocatalysis of (a, b) Rhd B, and (c, d) TC, using EDTA-NiMOF sample

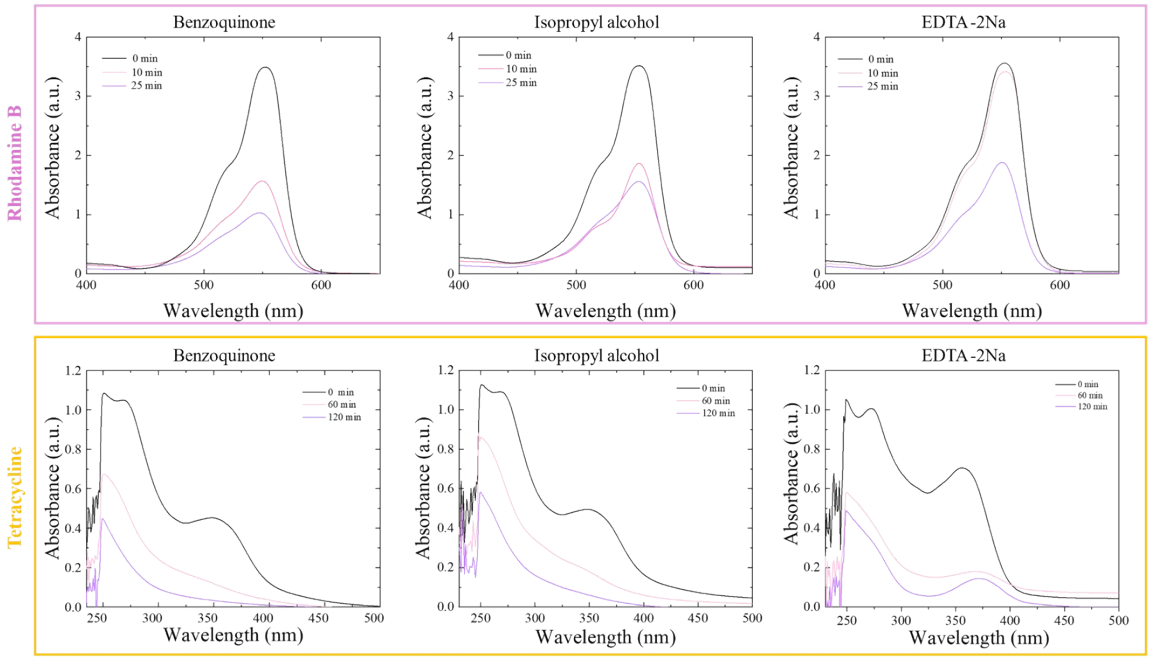

Fig. S8. UV-Visible plots for Scavenger tests conducted for EDTA-NiMOF sample.

DFT calculations

The DFT calculations were performed using the Gaussian 09W software package, employing the B3LYP functional with the 6-31G basis set. The convergence criteria were set with an energy threshold of 10^{-6} Hartree and a force convergence of 10^{-5} Hartree/Bohr to ensure accurate optimization. The charge and spin multiplicities for each complex, including TPA, EDTA, Ni-TPA, Ni-EDTA, and Ni-TPA-EDTA, were explicitly defined. The optimized structures, bond lengths, and bonding energy calculations have been incorporated in Figure S6, with the bonding energy equations (19)–(21) providing insight into the preferential formation of these complexes. Additionally, the adsorption energies for Rhodamine B (E_ads = -168.8 kcal/mol) and tetracycline (E_ads = -40.1 kcal/mol) were calculated to evaluate their interaction strength with the EDTA-

NiMOF complex, demonstrating that Rhd B binds more strongly, which may explain its higher photocatalytic degradation efficiency. To further support these findings, surface interaction visualizations comparing NiMg LDH and EDTA-NiMOF on the MgO substrate have been provided, illustrating the enhanced stability and surface interaction of EDTA-NiMOF. These additions ensure that all relevant computational parameters and theoretical insights are explicitly detailed, strengthening the scientific rigor of the manuscript. The optimized parameters of the simulated structures are presented in Table S2.

Table S2. Energy optimization values (Kcal/mol) for the studied structures.

Structure	Energy Optimization (Kcal/mol)
Ni (ion)	-946240.56
EDTA	-689664.43
TPA	-382272.58
Ni-2TPA	-1709304.8
Ni-EDTA	-1636369.36
TPA-Ni-EDTA	-2017543.79
Rhd B	-1180113.39
Rhd B. TPA-Ni-EDTA	-3197820.34
TC	-980044.506
TC. TPA-Ni-EDTA	-2997632.22

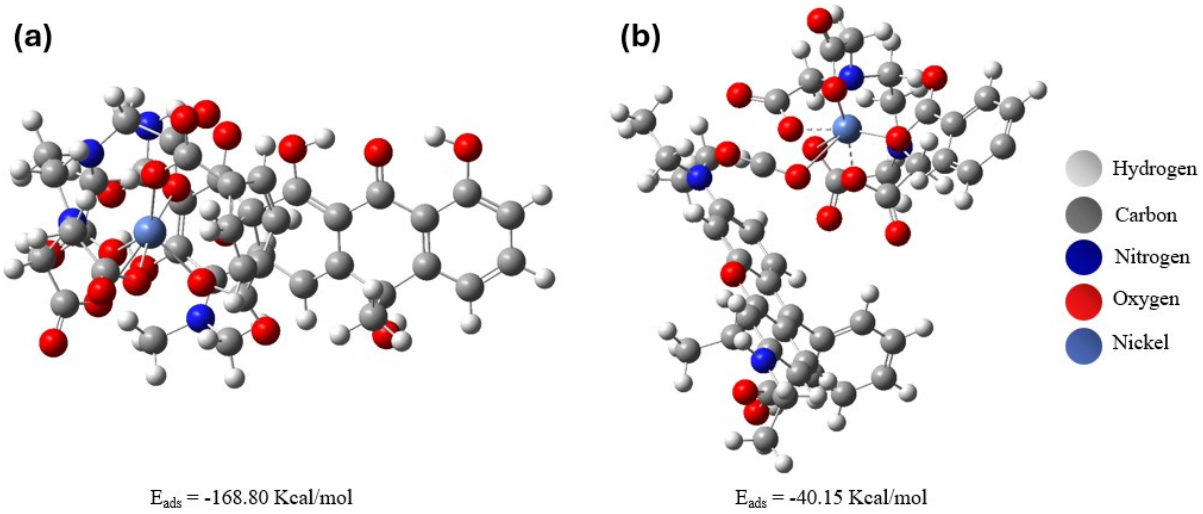

Fig. S9. DFT optimization and adsorption energy of the TPA-Ni-EDTA complex with (a) Rhd B, and (b) TC.